Jurnal Pharmascience, Volume 13, Issue 1, March 2026, page: 163-186
ISSN-Print 2355 – 5386
ISSN-Online 2460-9560
https://dx.doi.org/10.20527/jps.v13i1.24555
Research Article

Molecular Basis for the Enhanced CDK2 Inhibition by Artesunate: Superior Binding Affinity to the ATP-Catalytic Site

Dasar Molekuler untuk Peningkatan Inhibisi CDK2 oleh Artesunate: Afinitas Ikatan Superior ke Situs Katalitik ATP

Mohammad Rizki Fadhil Pratama [1]*, Evi Mulyani[1,2], Suratno[1,3], Punet Kumar[4], Daryono Hadi Tjahjono[5], Tutus Gusdinar Kartawinata[5]

[1]Pharmacy Department, Faculty of Pharmacy, Universitas Muhammadiyah Palangkaraya, Palangka Raya, Central Kalimantan, Indonesia
[2]Doctoral Program of Pharmacy, Faculty of Pharmacy, Universitas Ahmad Dahlan, Yogyakarta, Special Region of Yogyakarta, Indonesia
[3]Doctoral Program of Pharmaceutical Sciences, School of PhD Studies, Semmelweis University, Budapest, Central Hungary, Hungary
[4]Department of Pharmaceutical Chemistry, Shri Gopichand College of Pharmacy, Baghpat, India
[5]Pharmacochemistry Department, School of Pharmacy, Institut Teknologi Bandung, Bandung, West Java, Indonesia
Email: mohammadrizkifadhilpratama@umpr.ac.id

ABSTRACT

This study aimed to identify the most potent CDK2 inhibitor among seven artemisinin derivatives and, critically, to elucidate its binding mechanism and compare its affinity with that of the natural ligand, ATP. Molecular docking was performed using AutoDock 4.2.6 toward inactive and active forms of CDK2. Ligands were optimized using the Hartree-Fock method basis set 6-311G. Blind docking on the active form was used to determine the inhibition mechanism, employing the free energy of binding (ΔG) and dissociation constant (K_i) as affinity markers. Artesunate was the most potent derivative, exhibiting the highest affinity towards the active CDK2 form, with a ΔG of -11.7 kcal/mol and a K_i of 2.66 nM. Blind docking confirmed an ATP-competitive inhibition mechanism. Remarkably, Artesunate's K_i was significantly lower than that of ATP (8.73 nM). This enhanced affinity is attributed to specific interactions between the hemisuccinate side chain and the critical amino acid region, from 13-Gly to 16-Gly. Artesunate is suggested as a potent, ATP-competitive CDK2 inhibitor with an affinity exceeding that of ATP. These hypothesis-generating results suggest anticancer potential, yet require validation

via MD or assays; limitations like scoring bias and protein flexibility necessitate cautious interpretation regarding the 13-Gly to 16-Gly target.

Keywords: Artemisinin, Anticancer Agent, ATP, Molecular Docking, 13-Gly-16-Gly Loop

ABSTRAK

Penelitian ini bertujuan untuk mengidentifikasi inhibitor CDK2 paling poten di antara tujuh turunan artemisinin dan, yang terpenting, untuk menjelaskan mekanisme pengikatannya serta membandingkan afinitasnya dengan ligan alami, ATP. Penambatan molekuler dilakukan menggunakan AutoDock 4.2.6 terhadap bentuk CDK2 yang tidak aktif dan aktif. Ligan dioptimalkan menggunakan metode Hartree-Fock basis set 6-311G. Penambatan buta pada bentuk aktif digunakan untuk menentukan mekanisme penghambatan, dengan menggunakan energi bebas pengikatan (ΔG) dan konstanta disosiasi (K_i) sebagai penanda afinitas. Artesunat merupakan turunan paling poten, menunjukkan afinitas tertinggi terhadap bentuk CDK2 aktif, dengan ΔG -11,70 kkal/mol dan K_i 2,66 nM. Penambatan buta mengonfirmasi mekanisme penghambatan kompetitif ATP. K_i Artesunat secara signifikan lebih rendah daripada ATP (8,73 nM). Afinitas yang meningkat ini disebabkan oleh interaksi spesifik antara rantai samping hemisuksinat dan daerah asam amino kritis, dari 13-Gly hingga 16-Gly. Artesunat terkonfirmasi sebagai inhibitor CDK2 yang poten dan kompetitif terhadap ATP dengan afinitas yang melebihi ATP. Hasil penghasil-hipotesis ini menunjukkan potensi antikanker, namun memerlukan validasi via MD atau pengujian; batasan seperti bias fungsi skor dan fleksibilitas protein menuntut interpretasi hati-hati terkait target 13-Gly hingga 16-Gly.

Kata Kunci: Artemisinin, Agen antikanker, ATP, Penambatan molekuler, Loop 13-Gly-16-Gly

I. INTRODUCTION

Cancer is fundamentally driven by dysregulated cell cycle progression, making Cyclin-dependent kinases (CDKs) premier drug targets (Asghar et al., 2015). CDK2, in particular, is critical for the G_1/S phase transition, and its overexpression, often associated with Cyclin E amplification, confers resistance to CDK4/6 inhibitors like Palbociclib (Knudsen et al., 2025). While first-generation CDK inhibitors (e.g., Roscovitine) lacked selectivity and suffered from high toxicity, the field has progressed toward highly selective CDK2 inhibitors (e.g., BLU-222, INX-315) currently advancing through clinical trials (Zhang et al., 2021). This highlights the sustained therapeutic interest in CDK2 as a strategy to overcome treatment resistance and address *CCNE1*-driven tumors.

A major challenge in developing CDK2 selective agents is the high sequence and structural homology between the ATP-binding pockets of CDK2 and CDK1. This lack of difference has made the rational

design of specific competitive inhibitors difficult, often necessitating strategies like targeting allosteric pockets or leveraging minor, dynamic conformational differences (Faber et al., 2023; Jin et al., 2024). This complexity has renewed interest in repurposing natural products with established safety profiles and novel chemical scaffolds, such as the artemisinin class.

Artemisinin derivatives, famously known for their endoperoxide moiety and antimalarial activity, also exhibit potent cytotoxicity across various cancer cell lines (Crespo-Ortiz & Wei, 2012; Li et al., 2016; Wen et al., 2024). Their established anticancer mechanisms are multifaceted, involving the induction of oxidative stress (ROS) via iron interaction, promotion of apoptosis, and, critically, induction of G_1/S phase cell cycle arrest, suggesting interaction with CDK2 signaling (Barman et al., 2023; Firestone & Sundar, 2009; Kiani et al., 2020; Xia et al., 2025). However, despite preclinical success, the precise molecular interaction that leads to CDK2 inhibition, whether through competitive binding at the ATP site or via an allosteric mode, remains ambiguous in the literature.

To resolve this ambiguity and capitalize on the therapeutic potential of this drug class, we employed molecular docking to systematically screen artemisinin derivatives against CDK2. This study aims not only to identify the most potent derivative but also to conduct a high-resolution analysis of its mechanism. The unique contribution of this research is the direct, quantitative comparison of the lead compound's binding affinity (K_i) against the natural ligand ATP, identifying the specific amino acid interactions that confer superior affinity and providing a definitive structural blueprint for next-generation CDK2 inhibitor design.

II.METHOD

A. Ligands Preparation

For the computational study, the 3D chemical structures of the seven selected artemisinin derivatives: artemether (PubChem CID 643724), artemisinin (CID 68827), artemisone (CID 9891823), artemotil (CID 103986), artelinic acid (CID 153120), artesunate (CID 6917865), and dihydroartemisinin (CID 64965) were initially generated using the GaussView 3.08 (Gaussian, Inc). To accurately model the molecular conformation of the compounds in the absence of solvent, each structure was subjected to geometry optimization using the *ab initio* Hartree-Fock (HF) method with the 6-311G basis set, as implemented in the Gaussian 03 (Gaussian, Inc.). This rigorous optimization procedure yielded a reliable, minimized energy structure that approximates the

natural, most stable conformation (Bursch et al., 2022). Post-optimization, the resulting log files were converted to the standard PDB format utilizing Open Babel 3.1.0 (Muslimawati et al., 2025). Subsequently, the molecular docking simulations were carried out using AutoDock 4.2.6 (Hafid et al., 2024; Poerwono et al., 2024). This widely accepted freeware was chosen not only for its established history in producing crystal-structure-level accuracy in ligand placement but, crucially, for its predictive capacity for K_i, a key metric for guiding subsequent *in vitro* analyses (Castro-Alvarez et al., 2017). The final step in ligand preparation involved processing all molecules using AutoDockTools 1.5.6 (Forli et al., 2016), where Gasteiger charges were assigned and rotatable bonds (torsions) were defined, thereby yielding the finalized PDBQT file format necessary for the docking engine.

B. Receptors Preparation

The 3D atomic coordinates of CDK2 receptor were retrieved in PDB format from the RCSB Protein Data Bank database (http://www.rcsb.org). A comprehensive selection strategy was employed to ensure robust comparative analysis: instructures representing the inactive CDK2 conformation complexed with known inhibitors: JWS648, ANS-1, and ANS-2 (PDB ID 3PXZ), Roscovitine (PDB ID 2A4L), and SU9516 (PDB ID 3PY0) were obtained. The inactive forms were chosen specifically to compare the binding affinities and orientational patterns of the artemisinin derivatives against established CDK2 inhibitors (Anscombe et al., 2015). In parallel, the active CDK2 structure complexed with its natural ligand, ATP (PDB ID 1HCK), was retrieved. This active form was essential for the primary novelty of the study: quantitatively comparing the affinity of the selected artemisinin compound directly with ATP at the catalytic site (An et al., 2025). All proteins were prepared using AutoDockTools 1.5.6. Preparation involved standard steps: the removal of all irrelevant components (crystallographic water molecules and co-crystallized ligands), the addition of non-polar hydrogen atoms, and the assignment of Gasteiger partial charges. For targeted docking, the grid box size and coordinates were automatically determined by centering the grid on the position of the respective co-crystallized ligand (Arba et al., 2018), ensuring the grid fully enclosed the active/binding site being investigated (Table I).

Table I. Docking protocol of CDK2 receptors

PDB ID	Chain	Co-crystal Ligand	Grid Center (x, y, z)	Grid Size (x, y, z; Å)	GA Runs
3PXZ	A	JWS648	104.348 95.491 29.762	26 x 20 x 20	60
3PXZ	A	ANS-1	122.927 100.281 29.709	28 x 20 x 20	60
3PXZ	A	ANS-2	114.278 99.939 25.524	24 x 24 x 20	60
3PY0	A	SU9516	-92.139 79.537 85.219	60 x 60 x 60	60
2A4L	A	Roscovitine	100.203 101.649 79.938	60 x 60 x 60	60
1HCK	A	ATP	102.135 97.37 81.866	28 x 30 x 26	60

Table II. Blind docking protocol for 1HCK receptor

PDB ID	Chain	Grid Center (x, y, z)	Grid Size (x, y, z; Å)	Cluster distribution
1HCK	A	104.135 99.37 83.866	126 x 126 x 126	150

C. Validation of Docking Protocol

Prior to commencing the primary screening process, the utilized AutoDock 4.2.6 protocol was rigorously established for accuracy and reproducibility through a validation process. This step employed the re-docking method, where the co-crystallized ligand was initially extracted from the receptor and subsequently re-docked into its original binding pocket (Megantara et al., 2016). The core metric for assessing performance was the root mean square deviation (RMSD), which precisely quantifies the average positional difference between the predicted (re-docked) ligand atoms and the experimentally determined (crystallographic) ligand atoms (Castro-Alvarez et al., 2017). A smaller RMSD value indicates that the docking software accurately reproduces the crystal structure's binding orientation, signifying a reliable search and scoring function. The protocol was accepted as validated only if the RMSD score for the top pose was no more than 2.0 Å, the conventional threshold used to confirm the method's fitness for predicting novel ligand-binding poses (Ramírez &

Caballero, 2018). This successful validation step provides essential confidence in the accuracy of the subsequent screening and mechanistic binding analysis.

D. Molecular Docking

The molecular docking simulations for all test ligands were performed using the Lamarckian Genetic Algorithm (LGA) implemented in AutoDock 4.2.6. Consistent search parameters were applied across all runs to maintain comparability, including 60 independent genetic algorithm runs, a population size of 150, a maximum number of energy evaluations set at 2,500,000 (considered a medium setting for precision), and a maximum of 27,000 generations. The docking process was executed in two critical stages. The first stage involved targeted docking of all seven artemisinin derivatives against the inactive CDK2 structure, specifically utilizing grid boxes defined around the known catalytic (ATP) and the allosteric sites. This stage was designed as a rapid initial screen to identify the most potent inhibitor based on calculated binding affinity (Lu et al., 2016). The second stage involved the blind docking of the best-performing ligand against the active form of CDK2 (1HCK). At this stage, the grid box covered the entire receptor surface to accurately determine the preferred, unconstrained binding site, thereby confirming the definitive inhibition mechanism (Liang et al., 2020). The binding site was defined using an expansive grid box encompassing the entire receptor surface, ensuring inclusion of the known orthosteric pocket for comprehensive blind docking (Table II). Docking was validated by successful redocking of the co-crystallized ligand into its original pocket, ensuring the grid box dimensions and center coordinates were appropriate for the targeted site.

E. ADMET Prediction

To complement the pharmacological and safety profiles of the test ligands, their ADMET (Absorption, Distribution, Metabolism, Excretion, and Toxicity) properties were predicted according to the integrated protocol described in our previous study (Pratama et al., 2019). This approach used multiple ADMET prediction web servers to ensure comprehensive and reliable results. Initially, the chemical structures of all ligands were standardized and converted into canonical SMILES format using OpenBabel 3.1.1. Finally, the predictive outcomes were visualized graphically, adhering to the representation standards established by Sukardiman et al. (2020).

F. Data Analysis

Ligand affinity toward the receptor was primarily quantified using two standard parameters generated by the software: ΔG in kcal/mol and K_i in nM (Forli et al., 2016). A more negative ΔG and a proportionally lower K_i value quantitatively signify a higher ligand affinity for the binding site. To validate the structural predictions, the binding modes of the test ligands were compared with the co-crystallized ligands (Yang et al., 2022). Specifically, the interacting amino acid residues and the formation of hydrogen bonds were analyzed to assess the similarity of the interaction profile. A higher degree of overlap in the interacting residues suggests a higher probability that the test ligand shares a similar mechanism of action and inhibitory profile to the reference ligand (Du et al., 2016).

III. RESULTS AND DISCUSSION

The molecular docking protocol was first validated by re-docking co-crystallized ligands within the ATP-binding pocket of each receptor structure. This process enabled the accurate determination of the grid box coordinates and size necessary to encompass the active site (Miller et al., 2015). The re-docking procedure yielded RMSD scores ranging from 0.651 to 1.817 Å. These low RMSD values, with the docked pose almost perfectly stacked upon the crystallographic pose (as visualized in Figure 1), confirmed the reliability and validity of the selected protein structures and the docking parameters for further ligand screening (Ramírez & Caballero, 2018). Key validation parameters, including ΔG, Ki, interacting amino acid residues, and grid dimensions, are summarized in Table III.

Following geometry optimization of all test ligands (Table IV), the first stage of docking involved screening all seven derivatives against the three known binding pockets of an inactive CDK2 (PDB ID 3PXZ). AutoDock 4.2.6 was employed with 100 runs of the Lamarckian Genetic Algorithm to ensure high conformational sampling accuracy (Forli et al., 2016). For each compound, the pose exhibiting the most negative ΔG (best stability) and the lowest dissociation constant (K_i) was selected as the representative binding mode (Du et al., 2016). Comparative analysis of the results (Tables V to VII) revealed that Artesunate consistently exhibited the most favorable binding free energy and the lowest K_i at both the ATP-catalytic and Allosteric Site 1. Although Artelinic Acid showed the highest affinity for Allosteric Site 2, it was surpassed by Artesunate in subsequent blind docking analyses (Table VIII). Consequently, Artesunate was selected as the lead compound for further detailed mechanistic investigation.

Furthermore, Artesunate was prioritized due to its established clinical safety profile as an approved antimalarial drug, offering a significant advantage over Artelinic Acid, which remains in the preclinical phase (Liu et al., 2023). Notably, the blind docking of Artesunate against the active CDK2 form yielded an even more negative ΔG and lower K_i than any result with the inactive form, suggesting a preferable binding stability toward the active conformation.

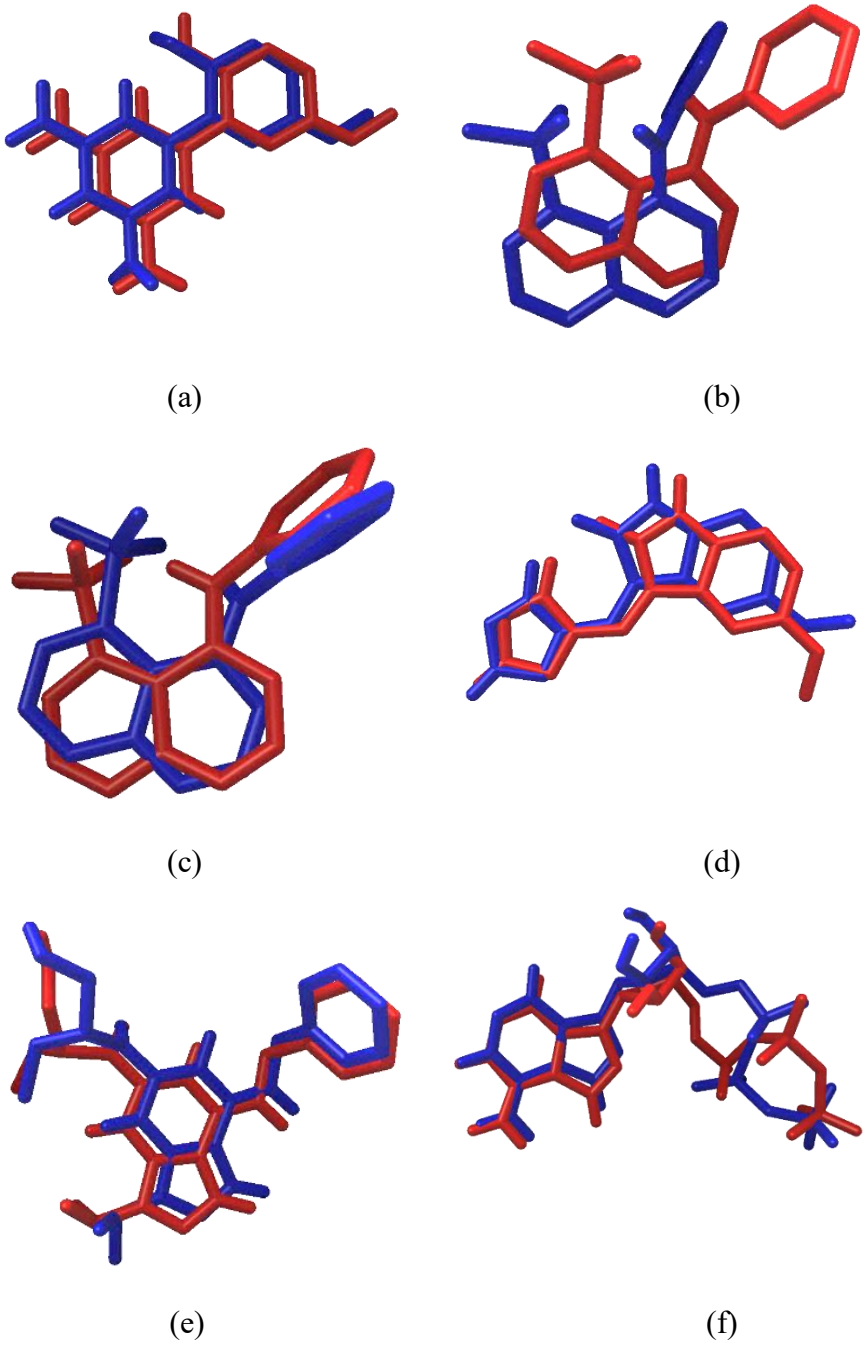

Figure 1. Validation results of CDK2 receptor and co-crystal ligands. JWS648, RMSD: 0.651 Å (a); ANS-1, RMSD: 1.817 Å (b); ANS-2, RMSD: 0.96 Å (c); SU9516, RMSD: 0.834 Å (d); Roscovitine, RMSD: 0.986 Å (e); ATP, RMSD: 0.874 Å(f). Blue: redocking results; Red: crystallography results

Table III. Validation results of CDK2 receptors

PDB ID	Ligand	RMSD (Å)	ΔG (kcal/mol)	K_i (nM)	Amino Acid Residues
3PXZ	JWS648	0.651	-5.75	61020	10-Ile, 31-Ala, 64-Val, 81-Glu, 83-Leu, 84-His, 86-Asp, 134-Leu, 144-Ala
3PXZ	ANS-1	1.817	-7.79	1940	35-Ile, 49-Ile, 52-Ile, 56-Lys, 69-Val, 76-Leu, 78-Leu
3PXZ	ANS-2	0.96	-8.94	281	15-Tyr, 33-Lys, 55-Leu, 56-Lys, 64-Val, 66-Leu, 78-Leu, 145-Asp, 146-Phe, 148-Leu
3PY0	SU9516	0.834	-7.51	3140	31-Ala, 64-Val, 80-Phe, 81-Glu, 82-Phe, 83-Leu, 84-His, 85-Gln, 134-Leu, 145-Asp
2A4L	Roscovitine	0.986	-7.2	5240	10-Ile, 31-Ala, 64-Val, 80-Phe, 81-Glu, 82-Phe, 83-Leu, 84-His, 85-Gln, 86-Asp, 89-Lys, 134-Leu, 144-Ala, 145-Asp
1HCK	ATP	0.874	-10.99	8.73	10-Ile, 13-Gly, 14-Thr, 18-Val, 31-Ala, 33-Lys, 81-Glu, 82-Phe, 83-Leu, 86-Asp, 129-Lys, 131-Gln, 132-Asn, 134-Leu, 145-Asp

Table IV. Structure of ligands

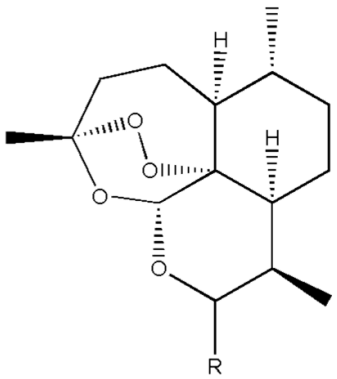

Ligands	R
Artemisinin	=O
Artemether	$-OCH_3$
Artemisone	$-N(CH_2)_4SO_2$
Artemotil	$-OCH_2CH_3$
Artelinic acid	$-OCH_2C(CH)_4CCOOH$
Artesunate	$-OCO(CH_2)_2COOH$
Dihydroartemisinin	-OH

Table V. Docking results of artemisinin derivatives at ATP-catalytic site of CDK2

Parameters	ART	ARM	ARO	ARL	ARA	ARS	DHA
ΔG (kcal/mol)	-8.26	-8	-4.64	-7.61	-7.72	-9.6	-8.5
K_i (nM)	880	1370	397790	2630	2200	91	590
Amino acid residues	10-Ile	10-Ile	10-Ile	10-Ile	10-Ile	10-Ile	10-Ile
	11-Gly	-	-	-	-	-	11-Gly
	12-Glu	-	-	12-Glu	-	12-Glu	-
	13-Gly	13-Gly	13-Gly	13-Gly	13-Gly	13-Gly	-
	18-Val	18-Val	18-Val	18-Val	18-Val	18-Val	18-Val
	31-Ala	31-Ala	31-Ala	31-Ala	31-Ala	31-Ala	-
	-	32-Leu	-	32-Leu	-	-	-
	33-Lys	33-Lys	33-Lys	33-Lys	33-Lys	33-Lys	-
	-	64-Val	64-Val	-	64-Val	-	-
	-	80-Phe	80-Phe	80-Phe	-	-	-
	83-Leu	-	83-Leu	-	83-Leu	83-Leu	83-Leu
	-	-	84-His	-	84-His	84-His	84-His
	85-Gln	-	85-Gln	-	85-Gln	85-Gln	85-Gln
	86-Asp	-	86-Asp	-	86-Asp	86-Asp	86-Asp
	134-Leu	134-Leu	134-Leu	134-Leu	134-Leu	134-Leu	134-Leu
	-	-	144-Ala	-	144-Ala	144-Ala	-
	-	145-Asp	145-Asp	-	145-Asp	-	-

Note: ART= Artemisinin; ARM= Artemether; ARO= Artemisone; ARL= Artemotil; ARA= Artelinic acid; ARS= Artesunate; DHA= Dihydroartemisinin; ΔG= Free energy of binding; Ki= Dissociation constant

Table VI. Docking results of artemisinin derivatives at allosteric site-1 of CDK2

Parameters	ART	ARM	ARO	ARL	ARA	ARS	DHA
ΔG (kcal/mol)	-6.02	-5.68	-4.89	-5.88	-7.35	-7.82	-5.75
K_i (nM)	38430	68530	262060	48780	4090	1850	60780
Amino acid residues	-	-	15-Tyr	-	-	-	-
	35-Ile	35-Ile	35- Ile	35-Ile	35-Ile	35-Ile	-
	37-Leu	-	37-Leu	-	-	37-Leu	37-Leu
	-	-	-	-	44-Val	-	-
	-	-	-	49-Ile	-	49-Ile	49-Ile
	52-Ile	52-Ile	52-Ile	52-Ile	52-Ile	52-Ile	52-Ile
	-	-	-	53-Ser	-	53-Ser	-
	56-Lys	56-Lys	56-Lys	56-Lys	56-Lys	56-Lys	56-Lys
	66-Leu	66-Leu	-	66-Leu	-	66-Leu	-
	69-Val	69-Val	69-Val	69-Val	69-Val	69-Val	69-Val
	71-His	71-His	71-His	71-His	71-His	-	71-His
	76-Leu	76-Leu	76-Leu	76-Leu	76-Leu	76-Leu	76-Leu
	78-Leu	78-Leu	78-Leu	78-Leu	78-Leu	78-Leu	-
	-	-	154-Val	-	-	-	-
	-	-	-	-	158-Val	-	-

Note: ART= Artemisinin; ARM= Artemether; ARO= Artemisone; ARL= Artemotil; ARA= Artelinic acid; ARS= Artesunate; DHA= Dihydroartemisinin; ΔG= Free energy of binding; Ki= Dissociation constant

Table VII. Docking results of artemisinin derivatives at allosteric site-2 of CDK2

Parameters	ART	ARM	ARO	ARL	ARA	ARS	DHA
ΔG (kcal/mol)	-7.98	-7.79	-6.08	-7.93	-10.27	-9.48	-8.13
K_i (nM)	1410	1940	35150	1550	30	110	1100
Amino acid residues	15-Tyr	15-Tyr	15-Tyr	15-Tyr	15-Tyr	15-Tyr	15-Tyr
	-	33-Lys	33-Lys	33-Lys	-	33-Lys	33-Lys
	-	-	35-Ile	-	-	-	-
	-	52-Ile	-	52-Ile	52- Ile	52-Ile	52-Ile
	55-Leu	55-Leu	55-Leu	55-Leu	55-Leu	55-Leu	55-Leu
	-	-	56-Lys	-	56-Lys	-	56-Lys
	63-Ile	-	63-Ile	-	-	-	-
	-	64-Val	64-Val	64-Val	64-Val	64-Val	64-Val
	66-Leu	66-Leu	66-Leu	66-Leu	66-Leu	66-Leu	66-Leu
	78-Leu	78-Leu	78-Leu	78-Leu	78-Leu	78-Leu	-
	80-Phe	80-Phe	80-Phe	80-Phe	80-Phe	80-Phe	80-Phe
	-	-	-	-	144-Ala	-	-
	-	145-Asp	145-Asp	145-Asp	-	145-Asp	145-Asp
	146-Phe	146-Phe	146-Phe	146-Phe	146-Phe	146-Phe	146-Phe
	-	-	148-Leu	-	148-Leu	148-Leu	-

Note: ART= Artemisinin; ARM= Artemether; ARO= Artemisone; ARL= Artemotil; ARA= Artelinic acid; ARS= Artesunate; DHA= Dihydroartemisinin; ΔG= Free energy of binding; Ki= Dissociation constant

Table VIII. Blind docking results of artemisinin derivatives at active form CDK2

Parameters	ART	ARM	ARO	ARL	ARA	ARS	DHA
ΔG (kcal/mol	-8.18	-8.14	-8.11	-8.73	-11.49	-11.7	-8.12
K_i (nM)	1010	1070	1140	400	3.33	2.66	1110
Amino acid residues	-	-	-	-	10-Ile	10-Ile	10-Ile
	-	-	12-Glu	-	12-Glu	-	-
	-	-	13-Gly	-	13-Gly	13-Gly	-
	-	-	-	-	14-Thr	14-Thr	-
	-	-	-	-	-	15-Tyr	-
	-	-	-	-	16-Gly	16-Gly	-
	18-Val	18-Val	18-Val	18-Val	-	18-Val	18-Val
	31-Ala	31-Ala	-	31-Ala	31-Ala	31-Ala	31-Ala
	-	-	-	32-Leu	-	-	-
	33-Lys	33-Lys	33-Lys	33-Lys	33-Lys	33-Lys	-
	-	64-Val	-	64-Val	-	-	64-Val
	80-Phe	80-Phe	80-Phe	80-Phe	-	80-Phe	80-Phe
	81-Glu	81-Glu	-	81-Glu	-	-	-
	-	82-Phe	-	82-Phe	82-Phe	82-Phe	82-Phe
	83-Leu	83-Leu	-	83-Leu	83-Leu	83-Leu	83-Leu
	-	-	-	-	86-Asp	-	-
	-	-	-	-	131-Gln	-	-
	-	-	-	-	-	-	132-Asn
	134-Leu	134-Leu	134-Leu	134-Leu	134-Leu	134-Leu	134-Leu
	144-Ala	144-Ala	144-Ala	144-Ala	144-Ala	144-Ala	144-Ala
	145-Asp	145-Asp	145-Asp	145-Asp	145-Asp	145-Asp	145-Asp

Note: ART= Artemisinin; ARM= Artemether; ARO= Artemisone; ARL= Artemotil; ARA= Artelinic acid; ARS= Artesunate; DHA= Dihydroartemisinin; ΔG= Free energy of binding; Ki= Dissociation constant

Table IX. Comparison of amino acid residues between docking results of artesunate

Parameters	Blind docking	ATP-catalytic site docking	Allosteric-1 site docking	Allosteric-2 site docking
Amino acid residues	**10-Ile**	**10-Ile**	-	-
	-	12-Glu	-	-
	13-Gly	**13-Gly**	-	-
	14-Thr	-	-	-
	15-Tyr	-	-	**15-Tyr**
	16-Gly	-	-	-
	18-Val	**18-Val**	-	-
	31-Ala	**31-Ala**	-	-
	33-Lys	**33-Lys**	-	**33-Lys**
	-	-	35-Ile	-
	-	-	37-Leu	-
	-	-	49-Ile	-
	-	-	52-Ile	52-Ile
	-	-	53-Ser	-
	-	-	-	55-Leu
	-	-	56-Lys	-
	-	-	-	64-Val
	-	-	66-Leu	66-Leu
	-	-	69-Val	-
	-	-	76-Leu	-
	-	-	78-Leu	78-Leu
	80-Phe	-	-	**80-Phe**
	82-Phe	-	-	-
	83-Leu	**83-Leu**	-	-
	-	84-His	-	-
	-	85-Gln	-	-
	-	86-Asp	-	-
	134-Leu	**134-Leu**	-	-
	144-Ala	**144-Ala**	-	-
	145-Asp	-	-	**145-Asp**
	-	-	-	146-Phe
	-	-	-	148-Leu

Note: Bold numbers indicates similar amino acid residues between blind and targeted docking

To confirm the mechanism of inhibition, the binding location of Artesunate from the blind docking on the active CDK2 form was compared to the pre-determined ATP-catalytic site. The comparison of interacting amino acid residues (Table IX) showed eight out of twelve residues (66.67%) in the ATP-catalytic site were also involved in Artesunate binding. This high degree of overlap confirms that Artesunate binds in a position highly analogous to the natural substrate, leading to the clear conclusion that Artesunate acts via an ATP-competitive inhibition mechanism (Law et al., 2015). This finding is consistent with

prior *in silico* and *in vitro* studies that have suggested ATP-competitive activity for other artemisinin derivatives (Crespo-Ortiz & Wei, 2012).

A key requirement for a successful ATP-competitive inhibitor is a binding affinity superior to that of the endogenous ligand, ATP. A direct comparison of the ARS blind docking result with ATP re-docking at the ATP-catalytic site was performed (Jug & Ilaš, 2025). AutoDock 4.2.6 predictions (Table X) yielded a ΔG of -11.70 kcal/mol and K_i of 2.66 nM for Artesunate; this surpasses the predicted Ki for ATP (8.73 nM), which was used as a standard benchmark for orthosteric binding. These values represent potential affinities in a rigid, Mg^{2+}-free receptor model and require experimental enzyme assays for definitive confirmation.

Although ATP interacted with a greater total number of amino acid residues (15 residues compared to 10 for Artesunate), the fewer, more selective interactions achieved by Artesunate resulted in a higher overall binding affinity (O'Neill et al., 2010). ATP serves as the natural substrate reference (positive control) to define the binding site and benchmark the docking scores of novel competitive inhibitors. Using ATP helps validate the grid parameters; if the software cannot re-dock ATP into its known crystal pose, the docking protocol for novel ligands is likely flawed. However, ATP's high number of rotatable bonds (10+) makes it a "moving target" that is notoriously difficult for algorithms to dock accurately without rigid constraints.

Visual inspection (Figure 2) revealed that the hemisuccinate side chain of Artesunate uniquely engages with the 13-Gly, 14-Thr, 15-Tyr, and 16-Gly loop region. This crucial side chain forms novel interactions not observed in the ATP binding mode, where ATP interactions in this region are limited to the beta and gamma phosphate groups engaging only 13-Gly and 14-Thr. Thus, the enhanced affinity of Artesunate is mechanistically attributed to the additional and essential non-covalent interactions established within the 13-16 amino acid loop.

To contextualize the inhibitory potential of Artesunate, its binding affinity was compared with that of several well-established ATP-competitive CDK2 inhibitors (Table XI). Artesunate yielded a more negative ΔG than Roscovitine, SU9516, and representatives from both aminopyrazole and oxindole inhibitor classes. This demonstrates that Artesunate possesses a higher calculated binding affinity than these inhibitors. While the affinity of Artesunate was slightly lower than that of the potent but non-selective inhibitor Staurosporine (less negative ΔG) (Rastelli et al., 2014), the data firmly

position Artesunate as a highly potent CDK2 inhibitor with significant potential for therapeutic development.

The comparative ADMET study (Figure 3) shows strong agreement among the six lipophilicity models (iLOGP to Consensus Log P), confirming that all seven ligands exhibit the hydrophobic nature required for efficient passive diffusion. While ARO and ARM occupy the highest lipophilic tier, they show an expected inverse relationship with the solubility parameters (ESOL, Ali Log S, and Silicos-IT LogSw), which are positioned closer to the chart's origin. Conversely, ARS and DHA exhibit improved water-solubility profiles, making them more versatile across different formulations while maintaining Log P values within the ideal "drug-like" range of 2.0 to 4.0 (Lee, 2020). The clustering of the "LOGP" and "Consensus LOG P" lines for ART and ARL suggests consistent pharmacokinetic behavior across different predictive algorithms for these specific scaffolds. Ultimately, the overlap of high absorption scores across the heptagonal axes indicates that all tested ligands are prime candidates for oral administration, with ARS providing the best balance between solubility and permeability.

Table X. Comparison of amino acid residues between docking results of artesunate

Parameters	ARS	ATP
ΔG (kcal/mol)	-11.7	-10.99
K_i (nM)	2.66	8.73
Amino acid residues	**10-Ile**	**10-Ile**
	13-Gly	**13-Gly**
	14-Thr	**14-Thr**
	15-Tyr	-
	16-Gly	-
	18-Val	**18-Val**
	31-Ala	**31-Ala**
	33-Lys	**33-Lys**
	80-Phe	-
	-	81-Glu
	82-Phe	**82-Phe**
	83-Leu	**83-Leu**
	-	86-Asp
	-	129-Lys
	-	131-Gln
	-	132-Asn
	134-Leu	**134-Leu**
	144-Ala	-
	145-Asp	**145-Asp**

Note: Bold numbers indicates similar amino acid residues between test and co-crystal ligands

Table XI. Comparison from ΔG of artesunate and known CDK2 inhibitors

PDB ID	RMSD (Å)	CDK2 inhibitors	ΔG of binding inhibitor (kcal/mol)	ΔG of binding artesunate (kcal/mol)
2A4L	0.986	Roscovitine	-7.2	-10
3PY0	0.834	SU9516	-7.51	-10.6
4EK5	0.731	Aminopyrazole	-9.83	-12.94
4ERW	0.723	Staurosporine	-11.75	-9.53
4FKQ	1.369	Oxindole	-9.69	-9.78

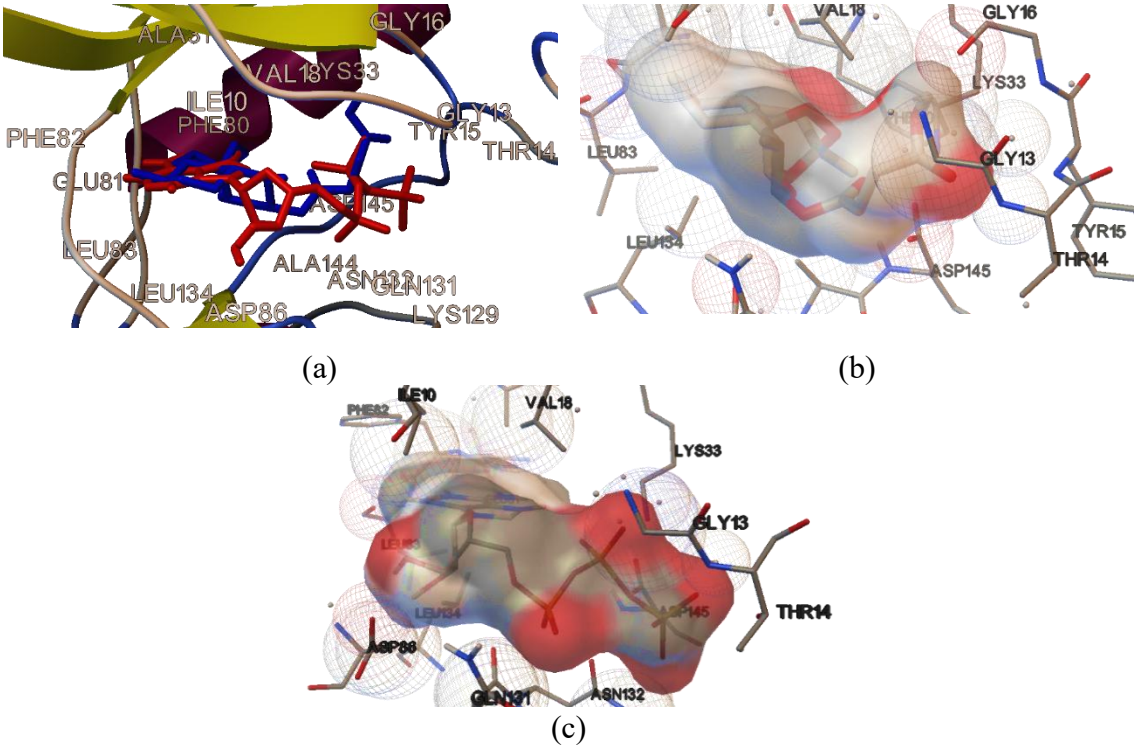

Figure 2. Overlay from blind docking of artesunate on CDK2 (blue) and redocking of ATP (red) (a); Interactions on blind docking results of artesunate on CDK2 (b); Interactions on redocking results of ATP on CDK2 (c)

The distribution analysis of the artemisinin derivatives reveals that the majority of ligands, particularly ARM and ARO, possess high BBB and CNS permeability scores. The radar chart highlights a strong correlation between lipophilicity and volume of distribution (VD_{ss}), with more hydrophobic compounds extending farther along the outer axes. Conversely, ARS shows a more restricted distribution in the central nervous system, likely due to its higher water solubility and different unbound fraction profile compared to its ether counterparts. Most test ligands exhibit relatively low "Fraction Unbound" scores, indicating they are highly bound to plasma proteins, which can influence their duration of action and half-

life (Tran et al., 2023). Overall, the consistent overlap in the distribution quadrants confirms that these ligands are highly effective at reaching target tissues, with DHA serving as a versatile central mediator in the group's pharmacokinetic profile.

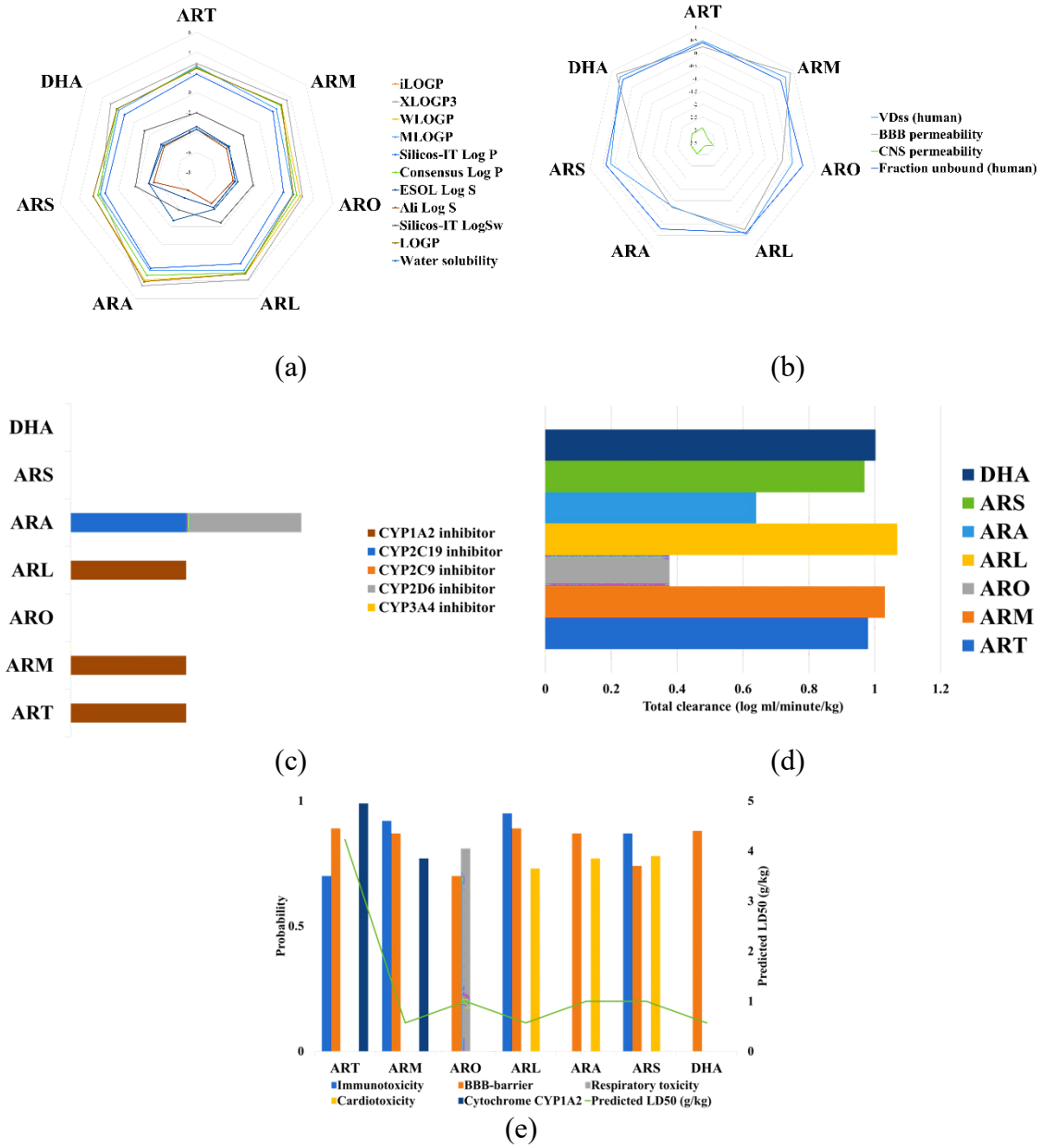

Figure 3. Prediction of parameters (a) absorption, (b) distribution, (c) metabolism, (d) excretion, and (e) toxicity of test ligands with SwissADME, pkCSM, and ProTox 3.0

The metabolism study reveals that all seven ligands are predominantly metabolized by CYP3A4, as reflected in the high overlap of scores along that axis. Most ARTs and their ether derivatives (ARM, ARO) exhibit low inhibition of CYP2D6 and CYP1A2, indicating a favorable safety profile for everyday drug-drug interactions (Hakkola et al., 2020). ARS stands out for its rapid biotransformation via esterases, resulting in a unique position on the radar chart that suggests a faster clearance rate than the more lipophilic analogs. The "Consensus Metabolism" scores for the group remain within the optimal boundaries, suggesting that these compounds do not significantly inhibit the liver's metabolic capacity (Lai et al., 2022). The high similarity in metabolic scores across the ARL, ARA, and DHA ligands highlights a shared chemical scaffold that yields predictable pharmacokinetic behavior in human hepatic models.

The excretion analysis shows that most artemisinin derivatives, particularly ARS, have high total clearance, minimizing the risk of long-term systemic accumulation. The radar chart indicates a strong link between water solubility and excretion rate, as the more hydrophilic ARS extends farther along the clearance axes than the more sequestered ARO. While ARM and ART show relatively synchronized clearance profiles, slight variations in their outer-ring positions reflect differences in metabolic stability before final excretion. The high total clearance scores across the entire group confirm that these compounds are efficiently removed from the body, supporting a favorable safety profile for repeated dosing (Wu et al., 2020).

The toxicity evaluation of these artemisinin derivatives as CDK2 inhibitors indicates that all seven ligands generally fall within the "safe" zone, characterized by high predicted LD_{50} values and low immunotoxicity potential (Ali et al., 2025). The chart shows that while ARM and ARO have superior BBB-barrier permeability, which helps target CDK2 in neuro-oncology, they also exhibit slightly elevated scores on the cardiotoxicity and respiratory toxicity axes compared to the parent ART. Interestingly, none of the ligands act as significant inhibitors of Cytochrome CYP1A2, suggesting a low risk of metabolic toxicity or interactions with co-administered drugs (Lee et al., 2024). ARS stands out as the least toxic candidate, likely because its rapid hydrolysis to DHA prevents prolonged systemic exposure that can lead to adverse respiratory effects. Ultimately, the high degree of overlap in the inner-most safety quadrants confirms that these ligands are promising CDK2 inhibitor candidates with

manageable toxicological profiles for further clinical exploration.

IV. CONCLUSION

The findings of this study demonstrate that among all tested artemisinin derivatives, Artesunate exhibited the highest binding affinity against CDK2, highlighting it as the most promising lead compound in this series. Furthermore, our detailed mechanistic analysis using blind docking unequivocally confirms that Artesunate functions as an ATP-competitive inhibitor at the CDK2 catalytic site. Critically, the computational data reveal that Artesunate possesses a quantitatively superior affinity to this binding site compared to the natural ligand, ATP. Structural insights suggest that key interactions involving the hemisuccinate side chain with residues in the 13-Gly to 16-Gly loop region are the critical determinants of this enhanced potency, providing a specific structural template for future ligand modification and optimization efforts. In light of these findings, the ADMET study further reinforces the therapeutic potential of Artesunate by revealing that it possesses the most favorable absorption and total clearance scores among the group, alongside the lowest predicted respiratory and immunotoxicity risks, making it the most pharmacokinetically viable candidate for CDK2 inhibition. Collectively, these robust computational results underscore the substantial therapeutic potential of Artesunate as a potent CDK2 inhibitor, meriting its accelerated preclinical development as a novel anticancer agent.

CONFLICT OF INTEREST

All authors declare that there is no conflict of interest in this research.

ACKNOWLEDGEMENT

This research was undertaken with the assistance of resources from the School of Pharmacy, Institut Teknologi Bandung, which is supported by the Institute for Research and Community Services, Universitas Muhammadiyah Palangkaraya.

REFERENCES

Ali, M. A., Sarker, H., Khan, T., Sheikh, H., Saif, A., Farid, F. Bin, Afrin, S., Khatun, M. A., & Kumar, N. (2025). Multi-omics pan-cancer profiling of CDK2 and in silico identification of plant-derived inhibitors using machine learning approaches. *RSC Advances*, *15*(44), 36938–36968. https://doi.org/10.1039/d5ra05535k

An, Q., Huang, L., Wang, C., Wang, D., & Tu, Y. (2025). New strategies to enhance the efficiency and precision of drug discovery. *Frontiers in Pharmacology*, *16*, 1550158. https://doi.org/10.3389/fphar.2025.1550158

Anscombe, E., Meschini, E., Mora-Vidal, R., Martin, M. P., Staunton, D., Geitmann, M., Danielson, U. H., Stanley, W. A., Wang, L. Z., Reuillon, T., Golding, B. T., Cano, C., Newell, D. R., Noble, M. E. M., Wedge, S. R., Endicott, J. A., & Griffin, R. J. (2015). Identification and Characterization of an Irreversible Inhibitor of CDK2. *Chemistry & Biology*, *22*(9), 1159–1164. https://doi.org/10.1016/j.chembiol.2015.07.018

Arba, M., Yamin, Y., Ihsan, S., & Tjahjono, D. H. (2018). Computational approach toward targeting the interaction of porphyrin derivatives with Bcl-2. *Journal of Applied Pharmaceutical Science*, *8*(12), 60–66. https://doi.org/10.7324/JAPS.2018.81208

Asghar, U., Witkiewicz, A. K., Turner, N. C., & Knudsen, E. S. (2015). The history and future of targeting cyclin-dependent kinases in cancer therapy. *Nature Reviews Drug Discovery*, *14*(2), 130–146. https://doi.org/10.1038/nrd4504

Barman, M., Dandasena, D., Suresh, A., Bhandari, V., Kamble, S., Singh, S., Subudhi, M., & Sharma, P. (2023). Artemisinin derivatives induce oxidative stress leading to DNA damage and caspase-mediated apoptosis in Theileria annulata-transformed cells. *Cell Communication and Signaling*, *21*, 78. https://doi.org/10.1186/s12964-023-01067-7

Bursch, M., Mewes, J., Hansen, A., & Grimme, S. (2022). Best-Practice DFT Protocols for Basic Molecular Computational Chemistry**. *Angewandte Chemie International Edition*, *61*(42), e202205735. https://doi.org/10.1002/anie.202205735

Castro-Alvarez, A., Costa, A., & Vilarrasa, J. (2017). The Performance of Several Docking Programs at Reproducing Protein–Macrolide-Like Crystal Structures. *Molecules*, *22*(1), 136. https://doi.org/10.3390/molecules22010136

Crespo-Ortiz, M. P., & Wei, M. Q. (2012). Antitumor Activity of Artemisinin and Its Derivatives: From a Well-Known Antimalarial Agent to a Potential Anticancer Drug. *Journal of Biomedicine and Biotechnology*, *2012*, 2475971. https://doi.org/10.1155/2012/247597

Du, X., Li, Y., Xia, Y.-L., Ai, S.-M., Liang, J., Sang, P., Ji, X.-L., & Liu, S.-Q. (2016). Insights into Protein–Ligand Interactions: Mechanisms, Models, and Methods. *International Journal of Molecular Sciences*, *17*(2), 144. https://doi.org/10.3390/ijms17020144

Faber, E. B., Sun, L., Tang, J., Roberts, E., Ganeshkumar, S., Wang, N., Rasmussen, D., Majumdar, A., Hirsch, L. E., John, K., Yang, A., Khalid, H., Hawkinson, J. E., Levinson, N. M., Chennathukuzhi, V., Harki, D. A., Schönbrunn, E., & Georg, G. I. (2023). Development of allosteric and selective CDK2 inhibitors for contraception with negative cooperativity to cyclin binding. *Nature Communications*, *14*(1), 3213. https://doi.org/10.1038/s41467-023-38732-x

Firestone, G. L., & Sundar, S. N. (2009). Anticancer activities of artemisinin and its bioactive derivatives. *Expert Reviews in Molecular Medicine*, *11*, e32. https://doi.org/10.1017/S1462399409001239

Forli, S., Huey, R., Pique, M. E., Sanner, M. F., Goodsell, D. S., & Olson, A. J. (2016). Computational protein–

ligand docking and virtual drug screening with the AutoDock suite. *Nature Protocols*, *11*(5), 905–919. https://doi.org/10.1038/nprot.2016.051

Hafid, A. F., Sari, D. K., Wardana, F. Y., Pratama, M. R. F., Tumewu, L., Ilmi, H., Permanasari, A. A., Nisa, H. K., & Widyawaruyanti, A. (2024). In silico Investigation of Caged Xanthone Compounds Isolated from *Cratoxylum sumatranum* Stem Bark against *Entamoeba histolytica* Enzymes. *Letters in Drug Design & Discovery*, *21*(12), 2423–2437. https://doi.org/10.2174/1570180820666230818140501

Hakkola, J., Hukkanen, J., Turpeinen, M., & Pelkonen, O. (2020). Inhibition and induction of CYP enzymes in humans: an update. *Archives of Toxicology*, *94*(11), 3671–3722. https://doi.org/10.1007/s00204-020-02936-7

Jin, Y., Lu, H., Ge, H., Hou, X., & Fang, H. (2024). Recent Development of CDK2 Inhibitors as Anticancer Drugs: An Update (2015–2023). *Pharmaceutical Fronts*, *06*(03), e195–e220. https://doi.org/10.1055/s-0044-1789577

Jug, A., & Ilaš, J. (2025). ATP-competitive inhibitors for cancer treatment – kinases and the world beyond. *RSC Medicinal Chemistry*, *16*(9), 4044–4067. https://doi.org/10.1039/D5MD00235D

Kiani, B. H., Kayani, W. K., Khayam, A. U., Dilshad, E., Ismail, H., & Mirza, B. (2020). Artemisinin and its derivatives: a promising cancer therapy. *Molecular Biology Reports*, *47*(8), 6321–6336. https://doi.org/10.1007/s11033-020-05669-z

Knudsen, E. S., Witkiewicz, A. K., Sanidas, I., & Rubin, S. M. (2025). Targeting CDK2 for cancer therapy. *Cell Reports*, *44*(8), 116140. https://doi.org/10.1016/j.celrep.2025.116140

Lai, Y., Chu, X., Di, L., Gao, W., Guo, Y., Liu, X., Lu, C., Mao, J., Shen, H., Tang, H., Xia, C. Q., Zhang, L., & Ding, X. (2022). Recent advances in the translation of drug metabolism and pharmacokinetics science for drug discovery and development. *Acta Pharmaceutica Sinica. B*, *12*(6), 2751–2777. https://doi.org/10.1016/j.apsb.2022.03.009

Law, M. E., Corsino, P. E., Narayan, S., & Law, B. K. (2015). Cyclin-Dependent Kinase Inhibitors as Anticancer Therapeutics. *Molecular Pharmacology*, *88*(5), 846–852. https://doi.org/10.1124/mol.115.099325

Lee, J., Beers, J. L., Geffert, R. M., & Jackson, K. D. (2024). A Review of CYP-Mediated Drug Interactions: Mechanisms and In Vitro Drug-Drug Interaction Assessment. *Biomolecules*, *14*(1), 99. https://doi.org/10.3390/biom14010099

Lee, M.-K. (2020). Liposomes for Enhanced Bioavailability of Water-Insoluble Drugs: In Vivo Evidence and Recent Approaches. *Pharmaceutics*, *12*(3), 264. https://doi.org/10.3390/pharmaceutics12030264

Liang, J.-W., Wang, M.-Y., Wang, S., Li, S.-L., Li, W.-Q., & Meng, F.-H. (2020). Identification of novel CDK2 inhibitors by a multistage virtual screening method based on SVM, pharmacophore and docking model. *Journal of Enzyme Inhibition and Medicinal Chemistry*, *35*(1), 235–244. https://doi.org/10.1080/14756366.2019.1693702

Liu, Y., Li, H., Luo, Z., Yu, Y., Yang, J., Zhang, M., Law, B. Y. K., Huang, Z., & Li, W. (2023). Artesunate, a new

antimalarial clinical drug, exhibits potent anti-AML activity by targeting the ROS/Bim and TFRC/Fe $^{2+}$ pathways. *British Journal of Pharmacology*, *180*(6), 701–720. https://doi.org/10.1111/bph.15986

Li, Z., Li, Q., Wu, J., Wang, M., & Yu, J. (2016). Artemisinin and Its Derivatives as a Repurposing Anticancer Agent: What Else Do We Need to Do? *Molecules*, *21*(10), 1331. https://doi.org/10.3390/molecules21101331

Lu, F., Luo, G., Qiao, L., Jiang, L., Li, G., & Zhang, Y. (2016). Virtual Screening for Potential Allosteric Inhibitors of Cyclin-Dependent Kinase 2 from Traditional Chinese Medicine. *Molecules*, *21*(9), 1259. https://doi.org/10.3390/molecules21091259

Megantara, S., Iwo, M., Levita, J., & Ibrahim, S. (2016). Determination of ligand position in aspartic proteases by correlating tanimoto coefficient and binding affinity with root mean square deviation. *Journal of Applied Pharmaceutical Science*, *6*(1), 125–129. https://doi.org/10.7324/JAPS.2016.600120

Miller, R. L., Thompson, A. A., Trapella, C., Guerrini, R., Malfacini, D., Patel, N., Han, G. W., Cherezov, V., Caló, G., Katritch, V., & Stevens, R. C. (2015). The Importance of Ligand-Receptor Conformational Pairs in Stabilization: Spotlight on the N/OFQ G Protein-Coupled Receptor. *Structure*, *23*(12), 2291–2299. https://doi.org/10.1016/j.str.2015.07.024

Muslimawati, K., Fakih, T. M., Akbar, N. H., Putra, A. M. P., & Isnani, N. (2025). Molecular Docking Analysis Of Phenolic and Flavonoid Compounds from Eichhornia Crassipes for Antidiabetic Activity Through Interaction with PPAR- γ (5Y2O) and A-Glucosidase (3TOP). *Jurnal Pharmascience*, *12*(2), 468–481. https://doi.org/10.20527/jps.v12i2.23583

O'Neill, P. M., Barton, V. E., & Ward, S. A. (2010). The Molecular Mechanism of Action of Artemisinin—The Debate Continues. *Molecules*, *15*(3), 1705–1721. https://doi.org/10.3390/molecules15031705

Poerwono, H., Sulistyowati, M. I., & Pratama, M. R. F. (2024). 6-aminomethylpinostrobin Derivatives as Anti-breast Cancer: In Silico Insight. *Egyptian Journal of Chemistry*, *67*(7), 71–81. https://doi.org/10.21608/ejchem.2024.233232.8707

Pratama, M. R. F., Poerwono, H., & Siswodiharjo, S. (2019). ADMET properties of novel 5- *O* -benzoylpinostrobin derivatives. *Journal of Basic and Clinical Physiology and Pharmacology*, *30*(6), 20190251. https://doi.org/10.1515/jbcpp-2019-0251

Ramírez, D., & Caballero, J. (2018). Is It Reliable to Take the Molecular Docking Top Scoring Position as the Best Solution without Considering Available Structural Data? *Molecules*, *23*(5), 1038. https://doi.org/10.3390/molecules23051038

Rastelli, G., Anighoro, A., Chripkova, M., Carrassa, L., & Broggini, M. (2014). Structure-based discovery of the first allosteric inhibitors of cyclin-dependent kinase 2. *Cell Cycle*, *13*(14), 2296–2305. https://doi.org/10.4161/cc.29295

Sukardiman, Ervina, M., Fadhil Pratama, M. R., Poerwono, H., & Siswodihardjo, S. (2020). The coronavirus disease 2019 main

protease inhibitor from Andrographis paniculata (Burm. f) Ness. *Journal of Advanced Pharmaceutical Technology & Research*, *11*(4), 157–162. https://doi.org/10.4103/japtr.JAPTR_84_20

Tran, T. T. Van, Tayara, H., & Chong, K. T. (2023). Recent Studies of Artificial Intelligence on In Silico Drug Distribution Prediction. *International Journal of Molecular Sciences*, *24*(3), 1815. https://doi.org/10.3390/ijms24031815

Wen, L., Chan, B. C.-L., Qiu, M.-H., Leung, P.-C., & Wong, C.-K. (2024). Artemisinin and Its Derivatives as Potential Anticancer Agents. *Molecules*, *29*(16), 3886. https://doi.org/10.3390/molecules29163886

Wu, F., Zhou, Y., Li, L., Shen, X., Chen, G., Wang, X., Liang, X., Tan, M., & Huang, Z. (2020). Computational Approaches in Preclinical Studies on Drug Discovery and Development. *Frontiers in Chemistry*, *8*, 726. https://doi.org/10.3389/fchem.2020.00726

Xia, Y., Shi, C., Lu, J., Zhu, Z., Li, M., Pan, Y., Huang, X., Zhang, L., & Liu, A. (2025). Artemisinin and Its Derivatives from Molecular Mechanisms to Clinical Applications: New Horizons Beyond Antimalarials. *International Journal of Molecular Sciences*, *26*(17), 8409. https://doi.org/10.3390/ijms26178409

Yang, C., Chen, E. A., & Zhang, Y. (2022). Protein–Ligand Docking in the Machine-Learning Era. *Molecules*, *27*(14), 4568. https://doi.org/10.3390/molecules27144568

Zhang, M., Zhang, L., Hei, R., Li, X., Cai, H., Wu, X., Zheng, Q., & Cai, C. (2021). CDK inhibitors in cancer therapy, an overview of recent development. *American Journal of Cancer Research*, *11*(5), 1913–1935. https://pubmed.ncbi.nlm.nih.gov/34094661/